Structure of *Thermus thermophilus* HB8 Aspartate Aminotransferase and Its Complex with Maleate[†,‡]

Tadashi Nakai,[§] Kengo Okada,[§,||] Shohei Akutsu,[§] Ikuko Miyahara,[§] Shin-ichi Kawaguchi,[⊥] Ryuichi Kato,[⊥] Seiki Kuramitsu,[⊥] and Ken Hirotsu*[,§]

Department of Chemistry, Graduate School of Science, Osaka City University, Sugimoto, Sumiyoshi-ku, Osaka 558-8585, Japan, and Department of Biology, Graduate School of Science, Osaka University, Toyonaka, Osaka 560-0043, Japan

Received August 18, 1998; Revised Manuscript Received December 1, 1998

ABSTRACT: The three-dimensional structures of pyridoxal 5′-phosphate-type aspartate aminotransferase (AspAT) from *Thermus thermophilus* HB8 and pyridoxamine 5′-phosphate type one in complex with maleate have been determined by X-ray crystallography at 1.8 and 2.6 Å resolution, respectively. The enzyme is a homodimer, and the polypeptide chain of the subunit is folded into one arm, one small domain, and one large domain. AspATs from many species were classified into aminotransferase subgroups Ia and Ib. The enzyme belongs to subgroup Ib, its sequence being less than 16% identical to the primary sequences of *Escherichia coli* , pig cytosolic, and chicken mitochondrial AspATs, which belong to subgroup Ia whose sequences are more than 40% identical and whose three-dimensional structures are quite similar with the active site residues almost completely conserved. The first X-ray analysis of AspAT subgroup Ib indicated that the overall and the active site structures are essentially conserved between the AspATs of subgroup Ia and the enzyme of subgroup Ib, but there are two distinct differences between them. (1) In AspAT subgroup Ia, substrate (or inhibitor) binding induces a large movement of the small domain as a whole to close the active site. However, in the enzyme of subgroup Ib, only the N-terminal region (Lys13−Val30) of the small domain approaches the active site to interact with the maleate. (2) In AspAT subgroup Ia, Arg292 recognizes the side chain carboxylate of the substrate; however, residue 292 of the enzyme in subgroup Ib is not Arg, and in place of Arg292, Lys109 forms a salt bridge with the side chain carboxylate. The thermostability of the enzyme is attained at least in part by the high content of Pro residues in the β-turns and the marked increase in the number of salt bridges on the molecular surface compared with the mesophilic AspAT.

The degradation of most amino acids starts with the transfer of their α-amino group to α-keto acids. This reaction, called transamination, is catalyzed by aminotransferases, which have PLP[1] as the prosthetic group. AspAT, one of the most important of these enzymes, catalyzes a reversible transamination reaction between the dicarboxylic α-amino and α-keto acids by a ping-pong bi-bi mechanism, and extensive studies on this enzyme have been carried out and reviewed (*1*−*3*).

AspATs from many species were classified into aminotransferase subgroup I (*4*), which was further subdivided into subgroups Ia and Ib (*5*). More than 40% amino acid sequence identities were observed among AspATs from *Escherichia coli*, yeast, chicken, pig, etc., and more than 40% among those from *Thermus thermophilus* HB8, *Bacillus* sp. YM-2 (*6*), and *Rhizobium meliloti* (*7*). The former AspATs belong to subgroup Ia and the latter to subgroup Ib, and there is ≤16% sequence identity between them (*5*). A number of X-ray crystallographic studies on AspATs of subgroup Ia have been performed to elucidate the structure, function, and catalytic mechanism of the enzymes: chicken mAspAT (*3*, *8*), chicken cAspAT (*9*), eAspAT (*10*−*12*), and pig cAspAT (*13*). However, neither the X-ray structure of AspAT in subgroup Ib nor that of thermostable AspAT has yet been determined.

X-ray studies on AspAT subgroup Ia showed that the enzymes are homodimers with a subunit molecular weight of about 45 000 and have very similar three-dimensional structures. The polypeptide chain of the subunit is folded into two domains (one small and one large domain). The

[†] This study was supported by a Grant-in-Aid for Scientific Research on Priority Areas from the Ministry of Education, Science, Sports and Culture of Japan (08214212 and 10146247) and a grant on Research for the Future Program from the Japan Society for the Promotion of Science.

[‡] Coordinates for tAspAT and tAspAT in complex with maleate have been deposited in the Brookhaven Protein Data Bank as entries 1BJW and 1BKG, respectively.

* To whom correspondence should be addressed: Department of Chemistry, Graduate School of Science, Osaka City University, Sugimoto, Sumiyoshi-ku, Osaka 558-8585, Japan. E-mail: hirotsu@sci.osaka-cu.ac.jp. Fax: +81-6-6605-3131.

[§] Osaka City University.

[||] Present address: Department of Molecular Biology, Graduate School of Biological Sciences, Nara Institute of Science and Technology, 8916-5 Takayama, Ikoma, Nara 630-0101, Japan.

[⊥] Osaka University.

[1] Abbreviations: PLP, pyridoxal 5′-phosphate; PMP, pyridoxamine 5′-phosphate; AspAT, aspartate aminotransferase; tAspAT, *Thermus thermophilus* HB8 AspAT; eAspAT, *Escherichia coli* AspAT; cAspAT, cytosolic AspAT; mAspAT, mitochondrial AspAT; ASA, accessible surface area; MIR, multiple isomorphous replacement; rms, root-mean-square; Tyr70*, asterisk indicates a residue from another subunit of the dimer unit.

10.1021/bi9819881 CCC: $18.00 © 1999 American Chemical Society
Published on Web 02/04/1999

active site pocket is formed at the subunit interface and the domain interface. The coenzyme, PLP, resides at the bottom of the active site pocket and forms a Schiff base with the catalytic Lys residue. Although the overall sequence identity among AspATs of subgroup Ia is around 40%, the active site residues are almost completely conserved.

According to the aligned amino acid sequences of subgroups Ia and Ib, most of the active site residues essential for catalysis seem to be conserved between the AspATs of subgroups Ia and Ib (*5*), but the residue which recognizes the distal carboxylate of the substrate (Arg292 in AspATs of subgroup Ia) is unknown in the AspATs of subgroup Ib. Further, some important residues which aid the catalytic action together with the essential residues may not be conserved. It is well-known that the AspATs of subgroup Ia show a large conformational change in the small domain versus the large domain to close the active site upon binding of the substrate. This induced fit phenomenon has been elucidated in detail (*3*, *9*−*14*) but not uncovered in AspAT in subgroup Ib.

Structure determination of tAspAT should help in understanding the role of the active site residues, the mechanism of substrate recognition, and the function of the mobile small domain in AspAT, and comparing three-dimensional structures between subgroups Ia and Ib provides some insight into the thermostability of the protein folding. Here we report the first X-ray crystallographic studies of PLP-type tAspAT in the open form and PMP-type tAspAT in complex with maleate in the closed form at 1.8 and 2.6 Å resolution, respectively.

MATERIALS AND METHODS

Crystallization and Data Collection. The expression of tAspAT by *E. coli*, the purification of the expressed enzyme, and the crystallization of its PLP form together with preliminary crystallographic analysis have been reported elsewhere (*5*, *15*). The tAspAT in the PLP form was crystallized by vapor diffusion using ammonium phosphate as the precipitant at pH 4.3 and belonged to space group $P2_12_12_1$ with the following cell dimensions: $a = 124.3$ Å, $b = 113.6$ Å, and $c = 61.62$ Å. There is one dimer in the asymmetric unit, and approximately 52% of the crystal volume is occupied by solvent. The native X-ray diffraction data set was collected to 1.8 Å resolution at 287 K on the BL6A station at the Photon Factory, KEK (Tsukuba, Japan), using an X-ray beam with a wavelength 1.0 Å and Fuji Imaging Plates with a screenless Weissenberg Camera (*16*). The data sets for the crystals soaked in 1 mM $HgCl_2$ and 1 mM mercurochrome were collected to 3.0 and 3.5 Å resolution at 287 K, respectively, with a Rigaku R-AXIS IIc imaging plate detector, using monochromated CuKα radiation (40 kV and 100 mA).

The PLP-type enzyme was converted to the PMP type by adding cystein sulfinate. A solution containing 10 mg/mL protein, 10 mM cystein sulfinate, 100 mM KCl, 50 μM PMP, and 2 mM HEPES (pH 7.0) was allowed to stand for 30 min at room temperature, and the excess cystein sulfinate was removed by Sephadex G-25. A droplet of 5 μL of protein solution [10 mg/mL, 40 mM maleate, 100 mM KCl, and 2 mM HEPES buffer (pH 7.0)] was mixed with an equal volume of reservoir solution [200 mM sodium acetate, 100 mM sodium citrate, and 16% polyethylene glycol 6000 (pH 6.5)] and equilibrated against 400 μL of reservoir solution at 20 °C to give crystals of PMP-type tAspAT in a complex with maleate. The space group of the complex crystals is also $P2_12_12_1$ but with the following cell dimensions: $a = 197.30$ Å, $b = 109.71$ Å, and $c = 80.25$ Å. There are two dimers in the asymmetric unit, and approximately 52% of the crystal volume is occupied by solvent. The X-ray diffraction data set for tAspAT−maleate was collected to 2.6 Å resolution at 287 K with an R-AXIS IIc detector. All data were processed and scaled using the programs DENZO and SCALEPACK (Table 1) (*17*).

Structure Determination. The molecular replacement method was not used to solve the structure of tAspAT of subgroup Ib, since the primary sequence is less than 16% identical to those of eAspAT, cAspAT, and mAspAT of subgroup Ia. The structure of tAspAT in the PLP form was solved by the MIR method, using two isomorphous data sets. The scaling of all data and map calculations were performed with the CCP4 program suite (*18*). The difference Patterson map calculations for $HgCl_2$ and mercurochrome allowed clear interpretation of two and four mercury sites, respectively. Refinement of the heavy atom parameters and calculation of the initial phases were performed with the program MLPHARE (*18*). The resulting MIR map has a mean figure of merit of 0.47 at a resolution of 15−3.5 Å. The map was significantly improved by the process of solvent flattening (*19*) and local 2-fold symmetry averaging (*20*) with the program DM (*18*). The mean figure of merit reached 0.71 with the same resolution range. The map was of good quality, and the model of one subunit (subunit A) was gradually built into the 3.0 Å map through several cycles of model building using the program O (*21*). That of the other subunit (subunit B) in the asymmetric unit was obtained by taking advantage of the local 2-fold axis.

The initial structure of PMP-type tAspAT in a complex with maleate was determined with AMoRe (*22*), using the previously determined structure of tAspAT in the PLP form as the search model. The model was constructed from the dimeric molecule, in which all the side chains and two PLPs were included. A rotational search followed by a Patterson correlation refinement using data from 15 to 4 Å resolution gave two distinct solutions, which resulted in translational solutions of two dimers in the asymmetric unit with an R_{factor} of 45.2%.

The structure of tAspAT in the PLP form was refined by simulated annealing and energy minimization with 2-fold noncrystallographic symmetry (NCS) restraints using the program X-PLOR (*23*, *24*), using X-ray data from 8 to 2.5 Å resolution. The entire structure, including the PLP molecule, was scrutinized by successively omitting 10 residue segments of the model from the phasing calculation and inspecting the map. Refinement by simulated annealing and rebuilding was alternated until no further improvements in structure and statistics were apparent with an R_{factor} of 24.1% and an R_{free} of 30.7%. At this stage, the restraint on 2-fold noncrystallographic symmetry was removed, and the entire molecule was refined to an R_{factor} of 21.7% and an R_{free} of 30.1%. The resolution was progressively increased to 1.8 Å, and after several rounds of refinement and manual rebuilding, R_{factor} and R_{free} were reduced to 25.7 and 27.5%, respectively. A $2F_o - F_c$ map displayed one large peak at

Table 1: Data Collection, MIR, and Refinement Statistics

crystal	native PLP type	maleate complex PMP type	$HgCl_2$	mercurochrome
diffraction data				
resolution (Å)	1.8	2.6	3.0	3.5
no. of reflections				
unique	74202	52952	17195	16235
total	149097	185800	–	–
completeness (%)	90.7	97.3	95.6	97.5
R_{merge}[a] (%)	7.5	10.9	6.8	8.6
MIR				
R_{diff}[b] (%)			13.3	7.0
phasing power[c]			1.6	2.0
no. of sites			4	2
refinement				
resolution limits (Å)	8.0−1.8	8.0−2.6		
R_{factor} (%)	0.215	0.197		
R_{free} (%)	0.269	0.238		
deviations				
bond lengths (Å)	0.013	0.011		
bond angles (deg)	1.7	1.6		
B factors				
avg main chains (Å^2)	18.9	21.9		
avg side chains (Å^2)	20.9	22.5		
avg cofactors (Å^2)	12.6	17.1		
avg waters (Å^2)	37.7	33.7		

[a] $R_{merge} = \Sigma_{hkl}\Sigma_i|I_{hkl,i} - \langle I_{hkl}\rangle|/\Sigma_{hkl}\Sigma_i I_{hkl,i}$, where I is the observed intensity and $\langle I\rangle$ is the average intensity for multiple measurements. [b] $R_{diff} = \Sigma||F_{PH}| - |F_P||/\Sigma|F_P|$, where $|F_{PH}|$ and $|F_P|$ are the derivative and native structure factor amplitudes, respectively. [c] Phasing power is the ratio of the root-mean-square (rms) of the heavy atom scattering amplitude and the lack of closure error.

the active site pocket of each subunit. The residual peak was assigned to a phosphate anion by considering the shape, size, and peak height, and possible interactions of this peak with the neighboring amino acid residues. Water molecules were picked up on the basis of the peak heights and distance criteria from the difference map. The water molecules whose thermal factors were >76 Å^2 (maximum thermal factor of the main chain) after refinement were removed from the list. Further model building and refinement cycles resulted in an R_{factor} of 21.5% and an R_{free} of 26.9%, using 72 271 reflections [$F_o > 2\sigma(F_o)$] between 8.0 and 1.8 Å resolution (Table 1). During the last step of the refinement, unambiguous water molecules were added when a high temperature factor was being used. The maximum thermal factor of water molecules was 89 Å^2. The final model comprises 2 × 382 residues (three C-terminal residues are not visible), two PLPs, two phosphate ions, and 308 water molecules. The overall structures of subunits A and B are essentially the same. The average thermal factors of the main chain atoms (N, Cα, C, and O) in the two subunits are 21.6 (subunit A) and 16.2 Å^2 (subunit B), reflecting the lower crystal packing effect on subunit A than on the subunit B.

The structure of PMP-type tAspAT in a complex with maleate was refined by simulated annealing and energy minimization (*23*, *24*). As the four subunits (subunits C−F) in the asymmetric unit form a dimer of dimers generating a tetramer with noncrystallographic 222 symmetry, we made use of strict NCS constraints on all non-hydrogen atoms in the early stage. This was replaced in the later stage by strong (500 kcal/Å^2) harmonic NCS restraints. When the R_{factor} was <27%, the coenzyme PLP was converted to PMP, and the substrate analogue maleate was introduced into peaks on a $2F_o - F_c$ map. Water molecules were picked on the basis of the peak heights and distance criteria from the difference map. The water molecules whose thermal factors were >59 Å^2 (maximum thermal factor of the main chain) after refinement were removed from the list. Further model building and refinement cycles resulted in an R_{factor} of 19.7% and an R_{free} of 23.8% using 49 354 reflections [$F_o > 2\sigma(F_o)$] between 8.0 and 2.6 Å resolution (Table 1). During the last step of the refinement, unambiguous water molecules were added even when a high temperature factor was being used. The maximum temperature factor of water molecules was 71.3 Å^2. The final model comprises 4 × 382 residues (three C-terminal residues are not visible), four PMPs, and 280 water molecules. The structures of four independent subunits are quite similar. The average thermal factors of the main chain atoms (N, Cα, C, and O) in four subunits are 21.0, 22.4, 23.2, and 21.0 Å^2.

Analysis of the stereochemistry with PROCHECK (*25*) showed that all the main chain atoms except Thr296 fall within the generously allowed regions of the Ramachadran plot for both structures. The 602 and 54 residues of the PLP-type enzyme are in the most favored region and the additionally allowed region, respectively, and 1206 and 110 residues of the PMP-type enzyme are in the most favored region and the additionally allowed region, respectively. On the basis of electron density maps, it is confirmed that the conformation of Thr296 is correct. Pro138, Pro192, and Pro195 assume cis conformations. We use subunit A in PLP- and subunit C in PMP-type enzymes as the reference standards for the open and closed forms of tAspAT, respectively, for comparisons with the AspATs in subgroup Ia. Figure 1 displays a Cα backbone tracing of tAspAT of subgroup Ib and eAspAT of subgroup Ia in ribbon model drawings.

RESULTS AND DISCUSSION

Primary and Secondary Structure. The primary sequence of tAspAT (*5*) was aligned versus that of eAspAT with the following procedure. (1) The main chain atoms of the conserved residues in the active sites between tAspAT and

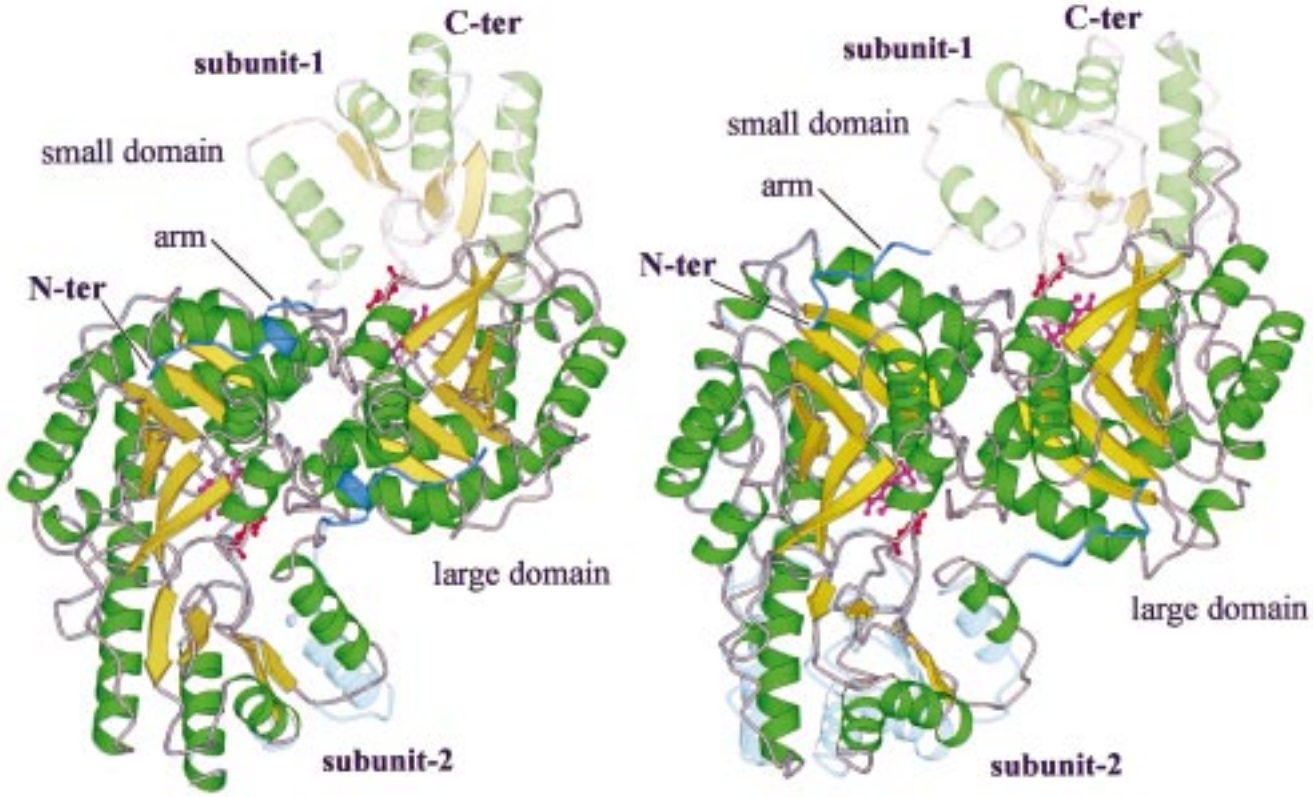

FIGURE 1: Cα ribbon tracing of tAspAT (left) and eAspAT (right) molecules viewed down the molecular 2-fold axis (*42*). The upper half of the molecule represents one subunit (subunit 1) in the closed form. The arm and α-helices and *β*-sheets of the large domain and those of the small domain are blue, green, yellow, pale green, and pale yellow, respectively. The lower half of the molecule is the superimposition of the other subunit (subunit 1) in the closed form onto that in the open form by least-squares fitting of Cα atoms in the large domain. The open form is light blue and the closed form green (α-helices) and yellow (*β*-sheets).

eAspAT are superimposed with a least-squares method. (2) Additional pairs of the amino acid residues were picked using the distance criteria and the conformational similarity using the program O (*21*). (3) The pairs found at step 2 were added to the residues used at the calculation of step 1, and the least-squares fitting of the main chain atoms was performed between tAspAT and eAspAT. (4) Steps 1 and 2 were repeated to give the sequence alignment of the AspATs of subgroup Ia and subgroup Ib as shown in Figure 2. The residues are numbered according to the sequence of pig cytosolic AspAT (*26*, *27*).

It is well-known that each subunit of AspAT in subgroup Ia is divided into two domains. The domain division was established for chicken mitochondrial AspAT (*3*, *8*) and more recently for pig cytosolic AspAT (*13*) on the basis of the correlated motion of the N-terminal and C-terminal parts of the polypeptide chain on inhibitor binding, resulting in essentially the same division. Although no correlated motion was observed in tAspAT, the division was adopted for convenience for tAspAT. The small domain is formed by two parts of the polypeptide chains from Lys13 to Asp48 and from Ala326 to the C-terminus and the large domain from Thr49 to Met325. The N-terminal part comprising Met2−Met12 is called an arm and does not belong to either domain. The arm, small, and large domains consist of 11 (8 in eAspAT), 127 (121), and 247 (267) residues, respectively.

The 385 amino acid residues of tAspAT are numbered from 2 to 411 with the deletion of 32, 34, and 43 residues and the insertion of 21, 18, and 16 residues in comparison with those of eAspAT, chicken mAspAT, and pig cAspAT, respectively (Figure 2). The main chain of the small domain is lengthened by five to eight residues and that of the large domain shortened by 22−31 residues compared with those of eAspAT, chicken mAspAT, and pig cAspAT. The insertion of 18, 17, and 16 residues and the deletion of 10, 10, and 11 residues are observed in the small domain, while only the deletion of 22, 24, and 31 residues in the large domain was observed. The insertion occurs only in the loop regions except for the N- and C-terminal regions, but the deletion occurs not only in the loop regions but also in the α-helices and *β*-strands.

The sequence identities of tAspAT with respect to eAspAT, chicken mAspAT, and pig cAspAT are 15.9, 13.6, and 13.1%, respectively. The corresponding values in the large domain are 17.9, 15.0, and 14.4%, which are significantly larger than 12.4, 11.0, and 10.8% in the small domain, suggesting that the primary sequence of the large domain is relatively well conserved between the AspATs of subgroups Ia and Ib, compared with that of the small domain. The sequences of both the small and large domains in tAspAT are more identical with those of eAspAT than with those of chicken mAspAT and pig cAspAT.

The subunit structure of PMP-type tAspAT−maleate is shown with secondary structure assignments from the program DSSP (*28*) in Figure 3. The AspATs of subgroup Ia so far determined by X-ray show almost common secondary structures except for a few additional short *β*-strands and one or two residue differences in the length of a few α-helices and *β*-strands (*13*). The arrangement of α-helices and *β*-sheets of tAspAT as a whole is similar to

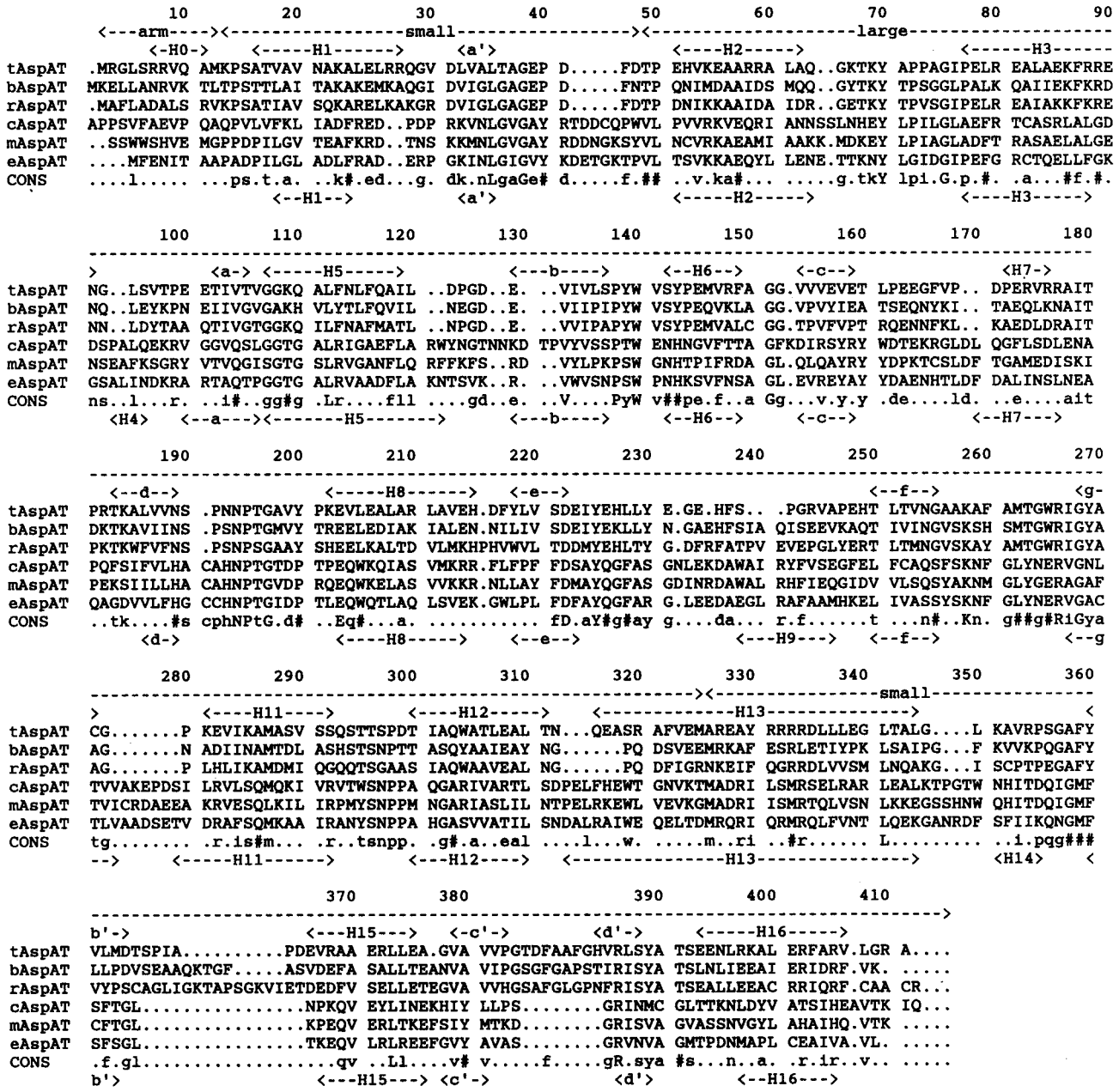

FIGURE 2: Alignments of six AspATs with secondary structure designations for tAspAT and eAspAT. α-Helices are denoted by H0−H16 and β-sheets by a−g in the large domain and a′−d′ in the small domain. tAspAT, bAspAT, and rAspAT are from *T. thermophilus* HB8, *Bacillus* sp. YM-2, and *R. meliloti*, respectively, and belong to subgroup Ib. cAspAT, mAspAT, and eAspAT are from pig cytosol, chicken mitochondria, and *E. coli*, respectively, and belong to subgroup Ia. In the consensus sequence, capital letters imply full conservation, small letters imply conservation in one of two groups, and # implies conservation in each subgroup.

those of the AspATs of subgroup Ia, indicating that the overall secondary structures of AspATs are conserved between subgroups Ia and Ib. However, a detailed comparison of secondary structures exhibits well-defined differences in the secondary structures. In tAspAT, the short α-helix H0 is observed in the arm, a three-stranded-like β-sheet is formed in the small domain, and α-helices H4, H9, and H14 are not found and change to parts of loops. The lengths of the α-helices, β-strands, and loops are considerably different between tAspAT and the AspATs of subgroup Ia.

Overall Structure. The overall structures of tAspAT and eAspAT are shown in Figure 1. The tAspAT is folded into a dimeric form ($M_r = 2 \times 42\,501$), and the Cα atoms of the two subunits are related by a noncrystallographic 2-fold axis. The overall structures of tAspAT and eAspAT are apparently similar, but are distinguishable. Especially, the N-terminal residues of the small domain between the arm and α-helix H1 exhibit a marked structural difference between tAspAT and eAspAT.

The large domain is an α/β-domain with an open twisted β-sheet structure. The seven β-strands designated a, g, f, e, d, b, and c (all parallel except for the g-strand) form a sharply twisted β-sheet structure as a central core surrounded by three α-helices (H5, H6, and H11) from the interior side of the protein and three α-helices (H3, H7, and H8) from the surface side (Figures 2 and 3). Many of the active site residues are situated at or near one end of a seven-stranded β-sheet (the C-terminus of a-, f-, e-, d-, and b-strands and the N-terminus of the g-strand), forming the base of the active site cavity. α-Helices H2 and H12 are located around the

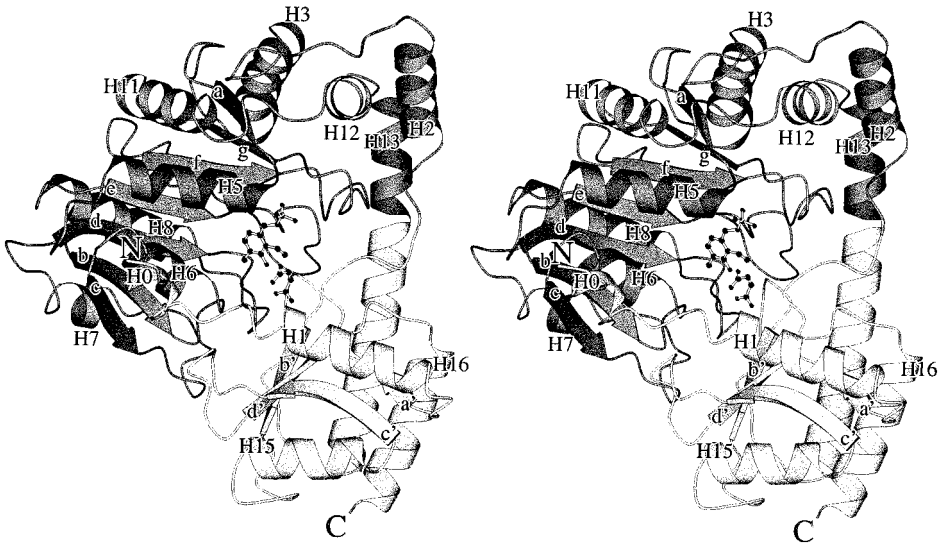

FIGURE 3: Stereoview of the subunit structure in PMP-type tAspAT−maleate with secondary structure assignments (*42*). α-Helices are denoted by H0−H16 and β-sheets by a−g in the large domain and a′−d′ in the small domain. The heavily shaded and lightly ribbons represent the large and the small domains, respectively.

Table 2: Molecular Surface and Subunit and Domain Interface

	tAspAT	eAspAT
ASA of dimer (Å^2)	27205	29397
nonpolar ASA of dimer (Å^2)	5461	5561
polar ASA of dimer (Å^2)	8149	12302
charged ASA of dimer (Å^2)	13595	11534
ASA of subunit interface (Å^2)	6011	6045
nonpolar ASA of subunit interface (Å^2)	1248	1604
polar ASA of subunit interafce (Å^2)	2710	2770
charged ASA of subunit interafce (Å^2)	2053	1671
ASA of domain interface (Å^2)	2775	2103
nonpolar ASA of domain interface (Å^2)	873	655
polar ASA of domain interface (Å^2)	1297	1171
charged ASA of domain interface (Å^2)	605	277
surface-to-volume ratio (Å^{-1})[a]	0.224	0.236
area of molecular surface (Å^2)	23368	25122
volume enclosed by molecular surface (Å^3)	104265	106302

[a] The surface-to-volume ratio is the ratio of the area of the molecular surface to the volume enclosed by the molecular surface.

molecular 2-fold axis, participating in the formation of the subunit interface.

The small domain also assumes an α/β-structure with a three-stranded-like β-sheet surrounded by four α-helices (H1, H13, H15, and H16) from the surface side of the small domain. The antiparallel β-sheet of three strands (b′, d′, and c′) is linked to the parallel β-sheet of two strands (c′ and a′) by sharing β-strand c′ to give the three-stranded-like β-sheet.

The ASAs of the molecule, the subunit interface, and the domain interface were calculated for the open forms of tAspAT and eAspAT (*11*) determined at 1.8 Å resolution as shown in Table 2 (*29*). The ASA of tAspAT is characterized by a relative increase (11%) in the charged area and a decrease (12%) in the polar area, in comparison with those of eAspAT. The ASA of the subunit interface is 6011 Å^2, which is comparable to the value of 6045 Å^2 in eAspAT. An increase in the charged area and a decrease in the nonpolar areas were observed on the subunit interface of tAspAT in comparison with those of eAspAT. The ASA of the domain interface in tAspAT is 670 Å^2 larger than that in eAspAT. This is due to the participation of the N-terminal region of the small domain in tAspAT in the domain interface. The charged area of the domain interface in tAspAT is twice that in eAspAT.

Open−Closed Conformational Change. One of the striking features of the AspATs in subgroup Ia is the overall enzymatic conformational change from the open to the closed form, depending on the binding of the substrates (*3*, *10*−*14*). This conformational change is due to the small domain movement to close the active site. Also in tAspAT of subgroup Ib, the binding of the inhibitor, maleate, induces a large conformational change from the open to the closed form. However, movement of the small domain as a whole was not observed, but only the N-terminal region from Lys13 to Val30 of the small domain approached to close the active site by changing the main chain dihedral angles around Gln28, Gly29, Val30, Asp31, and Leu32 (Figure 4). The Cα atoms of residues Met2−Met12 and Asp31 to the C-terminus in the open and the closed forms were superimposed by least-squares fitting with an rms deviation of 0.32 Å with a maximum displacement of 1.2 Å. In contrast to the good agreement of the Cα atoms of these residues, large differences from 3.3 (Lys13) to 8.2 Å (Ala19) were observed for residues Lys13−Val30. The Cα atoms of α-helix H1 (Ala16−Arg27b) of the open and the closed forms were fitted with an rms deviation of 0.44 Å with a maximum displacement of 0.73 Å (Thr17), indicating that α-helix H1 does not show a large conformational change and behaves like a rigid body on binding of the inhibitor. α-Helix H1, which is approximately parallel to α-helix H15, changes its direction to make its helical axis parallel to β-strands a′ and c′ and moves to the active site center, resulting in the direct interaction of its N-terminal residue Thr17 with the inhibitor. Concurrently, residues Lys13−Ala16 approach within 3.3−6.8 Å the active site with a large change in the main chain conformation to cover the entrance of the active site. Attention should be called to the conformational change in tAspAT on binding of the inhibitor because the packing interactions might affect the movement of the small domain. The tetramer found in the crystal of tAspAT−maleate was formed by the interactions between the large domains of two dimers; the small domains are not involved in the dimer−

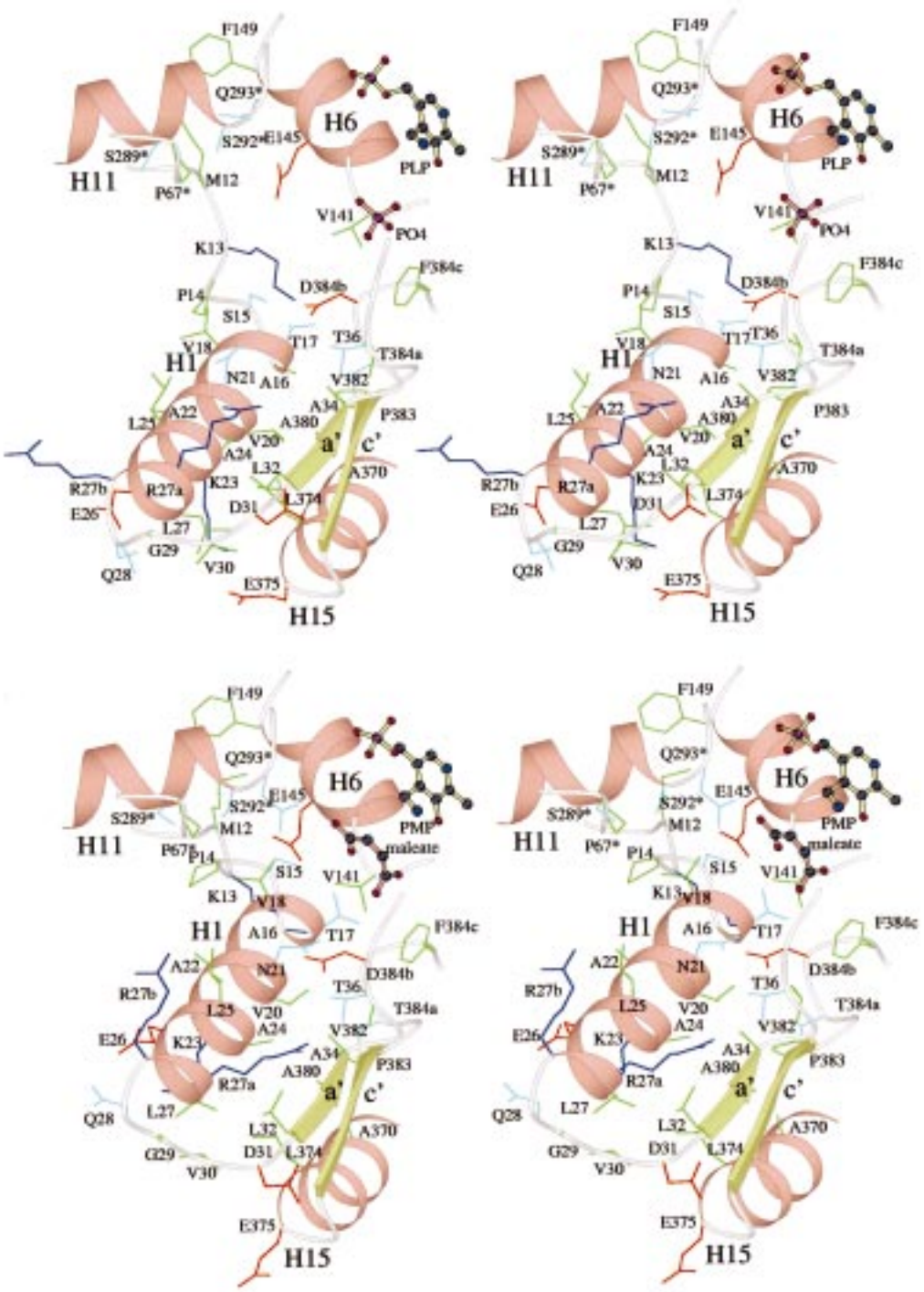

FIGURE 4: Stereodiagrams showing the large movement of the N-terminal region (Lys13−Val30) bearing α-helix H1 in the conformational change from the open (a, top) to the closed (b, bottom) forms (*42*). The viewing direction is the same as that in Figure 1. The N-terminal moving region and the part of the protein adjacent to it are shown. The side chains of the amino acid residues are green (hydrophobic), light blue (hydrophilic), purple (positively charged), and red (negatively charged) lines, and cofactors, phosphate ion, and maleate bound to the active site are shown as ball-and-stick models. Only α-Helix H1 (Ala16−Arg27b) and its terminal loops (Lys13−Ser15 and Gln28−Val30) of the small domain move toward the active site region.

dimer interactions, implying that the formation of a tetramer in the crystal does not affect the open−closed conformational change. The small domains of a tetramer were involved in interactions among tetramers in the crystal lattice, but the crystallographic environment around each small domain in a tetramer is different. The crystal of tAspAT−maleate was formed with the cocrystallization method. Thus, the conformational change found in the crystal might reasonably occur in solution.

In the open form of tAspAT, the side chains of Val20, Ala24, and Leu27 and the methylene moieties of the side chains of Lys23 and Arg27a arranged on one side of α-helix H1 interact with the side chains of Leu32 and Ala34 on β-strand a′, Ala370 and Leu374 on α-helix H15, and Ala380 on β-strand c′ to form a hydrophobic cluster. The side chains of the residues on the other side of α-helix H1 and Pro14 face the solvent region. The NH_3^+ of Lys13, OH of Ser15, and OH of Thr17 interact with the carboxylate of Asp384b.

On binding of the inhibitor, the hydrophobic residues on the one side of α-helix H1 are rearranged to form a new hydrophobic cluster with Leu32, Ala34, Leu374, Ala380, and Val382, and Ser15 and Thr17 in the N-terminal region of α-helix H1 switch interactions with Asp384b with the inhibitor, maleate, while the interaction between Lys13 and Asp384b is maintained. The main chain NH and C═O of Lys13 form hydrogen bonds with OE1 of Glu145 and NE2 of Gln293*, respectively, and Pro14 covers the part of the entrance of the active site pocket. Val18 and Asn21, which face the solvent region in the open form, partially cover the maleate from the solvent region with the side chain of Asn21 forming hydrogen bonds with the hydroxyl and carbonyl group of Thr36. α-Helix H1 slides on the surface comprising hydrophobic residues of β-strands a′ and c′ and α-helix H15 toward the active site (Figures 3 and 4). Thus, the movement of α-helix H1 is attained by a shear motion (*30*).

The ASAs of tAspAT are 27 205 and 26 288 Å^2 in the open and closed forms, respectively. The ASA is decreased by 458 Å^2 per subunit upon substrate binding, which is due to the large movement of the N-terminal part toward the active site. Especially, the stretch from Lys13 to Val18 greatly contributes to this change in ASA, because the buried ASA of this stretch into the protein interior by the active site closure was 231 Å^2 , of which 151 Å^2 is hydrophobic and 80 Å^2 is hydrophilic. The AspATs of many vertebrate enzymes and eAspAT have the consensus sequence of H14-X15-H16-H17-H18, where H represents the hydrophobic residue at the N-terminal region (*13*). This sequence, called a hydrophobic plug, is Pro14-Val15-Leu16-Val17-Phe18, Pro14-Asp15-Pro16-Ile17-Leu18, and Ala14-Asp15-Pro16-Ile17-Leu18 in pig cAspAT and chicken mAspAT and eAspAT, respectively. The ASA of the consensus sequence in pig cAspAT is buried 222 Å^2 into the protein interior in the domain closure. The main driving force for the change from the open to closed form was ascribed to the entropy-driven burial of these hydrophobic residues concurrent with the charge compensation of the two Arg residues in the active site by substrate binding (*13*). Also in tAspAT, the quasi-consensus sequence of Pro14-Ser15-Ala16-Thr17-Val18 exists, but this sequence is less hydrophobic than those of subgroup Ia; Ser15, Thr15, and Lys13 participate in many hydrogen bonds with the residues of the active site in the closed form. Thus, in tAspAT, not only the hydrophobic force but also hydrophilic interactions might play important roles in the active site closure.

The ASA of the domain interface in tAspAT is significantly larger than that in eAspAT, with the marked increase in the charged area of the domain interface in tAspAT (Table 2). There are nine salt bridges (distance cutoff of 4.0 Å) and 14 charged−neutral and seven neutral−neutral hydrogen bonds (distance cutoff of 3.5 Å) which bridge the large and small domains in the open form of tAspAT, while zero salt bridges and eight charged−neutral and four neutral−neutral hydrogen bonds are observed in eAspAT. The domain closure in AspATs of subgroup Ia appears to be a rigid body rotation of the small domain but, in fact, is caused by a series of small conformational changes over the domain interface (*8*). The tAspAT does not show the domain closure as was observed in the eAspAT of subgroup Ia. This is at least in part due to the differences in areas and properties of the domain interfaces between tAspAT and eAspAT.

Active Site of PLP−Type tAspAT in the Open Form. The stereo structure and hydrogen-bonding scheme of the active site are shown in Figures 5a and 6a, respectively. The molecule has two active site pockets around the molecular 2-fold axis. Each pocket is located at the domain interface of one subunit and at the subunit interface. The residues comprising the pocket are made up of three parts. The first part is the bottom of the active site pocket, which consists of residues Gly108 (Gly in eAspAT), Lys109 (Thr), Trp140 (Trp), Val141 (Pro), Ser142 (Asn), Tyr143 (His), Asn189 (His), Asn194 (Asn), Asp222 (Asp), Ile224 (Ala), Tyr225 (Tyr), Ala257 (Ser), Lys258 (Lys), and Arg266 (Arg), and is at one end of the seven-stranded β-sheet of the large domain. The second part forms a lid and one side of the active site pocket. The lid is formed by Ser15 (Asp), Ala16 (Pro), Thr17 (Ile), and Val18 (Leu) which have no direct interaction with the active site residues in the open form. One side of the active site wall consists of Thr36 (Gly), Ala37 (Ile), Gly38 (Gly), Tyr360 (Phe), and Arg386 (Arg) from the small domain of the same subunit. The first and second parts belong to the large and the small domains of the same subunit, respectively. The third part forms the other side of the active site pocket, which consists of residues Tyr70* (Tyr), Ser292* (Arg), Gln293* (Ala), and Thr296* (Ser) from the large domain of the other subunit. PLP is bound to this pocket by extensive noncovalent inteactions with the residues forming the bottom of the active site pocket except for Tyr70* and by forming an internal aldimine bond (Schiff base linkage) with catalytic residue Lys258. The internal aldimine bond (Schiff base, C4′═N) formed by PLP and Lys258 forms an angle of 46° with the pyridine ring of PLP. This angle is in fair agreement with the angles of 55 and 64° observed in eAspAT (*10*, *11*). The negative charge of the phosphate group is well balanced with the positive charge of Arg266 and the dipole of α-helix H5, whose N-terminus is close to the phosphate group. The phosphate ion and 12 water molecules are located in the active site and are involved in the formation of extensive hydrogen bonds as shown in Figures 5a and 6a. The phosphate anion occupies the binding region of the substrate α-carboxylate in the closed form, and its two oxygen atoms form a salt bridge with the guanidino group of Arg386 by end-on symmetric geometry (*31*). This salt bridge is rigidly fixed by Thr36 and W5 from one side and by Asn194 and Trp140 from the other side. In addition to this salt bridge, Arg386 forms a hydrogen bond with OD1 of Asn194, and the nonpolar segment of Arg386 undergoes van der Waals interaction with Phe360. The protonated N1 and O3$^-$ atoms of PLP form a salt bridge with the carboxylate of Asp222 and hydrogen bonds with Asn194 and Tyr225, respectively. The pyridine ring of PLP is sandwiched by the ethyl group of Ile224 (the methyl group of Ala in eAspAT) and the indole ring of Trp140. The pyridine ring of the cofactor is nearly parallel to the indole ring of Trp140 with an inclination angle of 6.1° between them, while in eAspAT, the arrangement of these two rings considerably deviates from the parallel orientation with a corresponding inclination angle of 20° (*10*, *11*). On the left side of the cofactor and phosphate (Figures 5a and 6a), there is an intricate hydrogen bond network starting from the phosphate moiety of the cofactor to Ser292*. The OH of Thr296*, NH_3^+ of Lys109, W1, and W2 form a cyclic hydrogen-bonding ring. This ring is

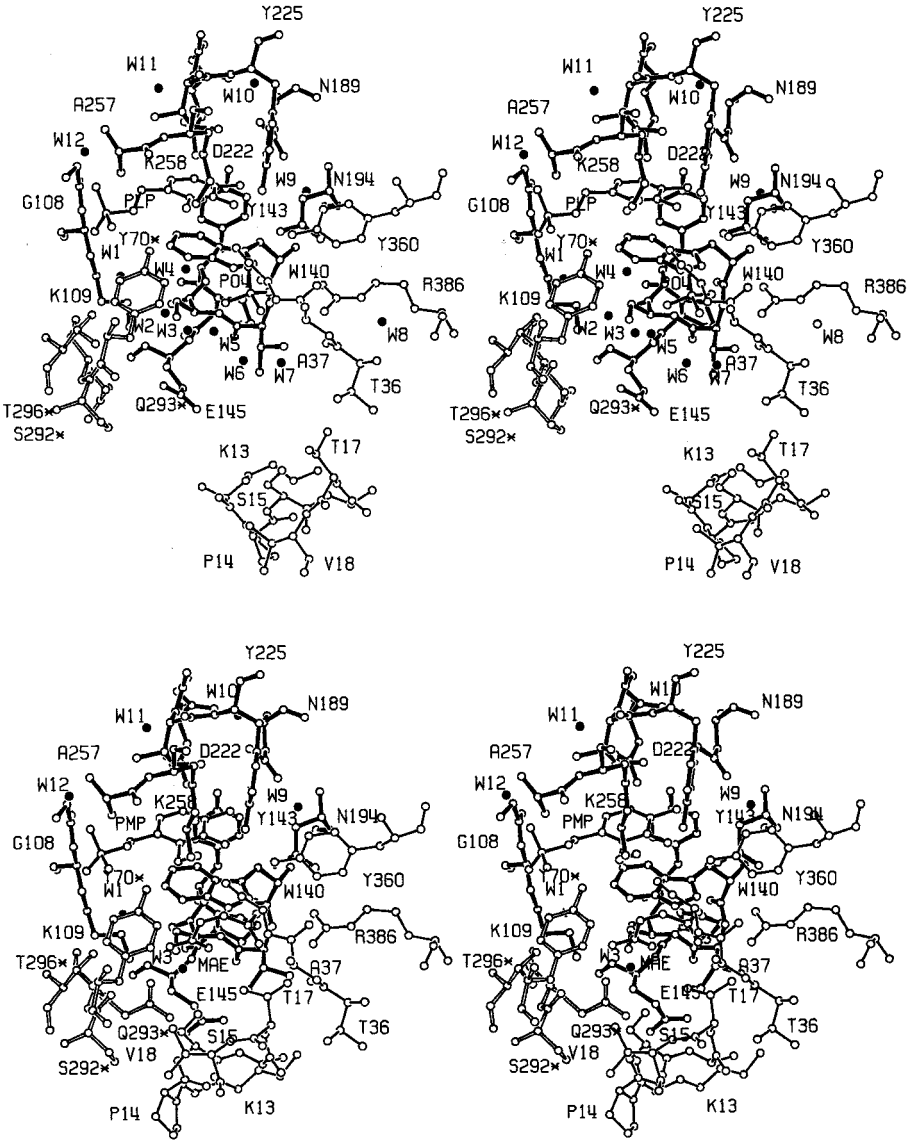

FIGURE 5: Stereodiagrams of the active sites of tAspAT in the open (a, top) and the closed (b, bottom) forms (*43*). Cofactors, phosphate ion, and maleate are represented by full bonds and waters by solid circles. Thick full bonds indicate the active site residues from the large domain of one subunit, thin lines those from the small domain of the same subunit, and thick open bonds those from the large domain of the other subunit.

connected to the phosphate moiety of the cofactor through W1, to the main chain C═O of Ser292* through NH_3^+ of Lys109, and to W3 and W4 through W2. W4 interacts with the phosphate anion and the phosphate moiety of the cofactor. W3 is further hydrogen-bonded to the OH of Ser142.

Active Site of PMP-Type tAspAT−Maleate in the Closed Form. The stereo structure and hydrogen-bonding scheme of the active site in the closed form are shown in Figures 5b and 6b. The binding of the maleate liberates six water molecules and the phosphate anion from the substrate binding region of the active site in the open form, inducing the access of the N-terminal region bearing the lid (Ser15-Ala16-Thr17-Val18) to the active site. Thus, the hydrogen bond networks around the maleate binding region are reconstituted. However, the active site residues except for Glu145, Gln293*, and the residues of the lid do not change their positions and retain the interactions among them on maleate binding, because the corresponding residues in the open and closed forms are superimposed within 0.85 Å except for the side chain of Lys258. Glu145 and Gln293* change their side-chain directions to form hydrogen bonds with the main chain NH and C═O of Lys13, respectively, suggesting that these interactions play some roles in the open−closed conformational change. N-Terminal residues Ser15, Thr17, and Val18 cover the entrance of the active site pocket to shield the maleate from the solvent. The average isotopic thermal factor of Pro14−Val18 is reduced by 36 $Å^2$ compared with that in the open form. One carboxylate of the maleate corresponding to the α-carboxylate of the substrate interacts with the active site residues just like the phosphate anion (P, O2, and O4) in the open form. The carboxylate and Arg386 form a salt bridge, which is fixed by the hydrogen-bonding interactions from both sides of the salt bridge, showing that the interactions of α-carboxylate of the substrate with the active site residues are essentially the same between tAspAT and AspATs of subgroup Ia. The other carboxylate of the maleate corresponding to the side chain carboxylate of the substrate participates in one salt bridge and four hydrogen bonds. One carboxylate oxygen (Ob in Figure 6b) of the maleate takes the place of W2 in the hydrogen-bonding cycle formed by

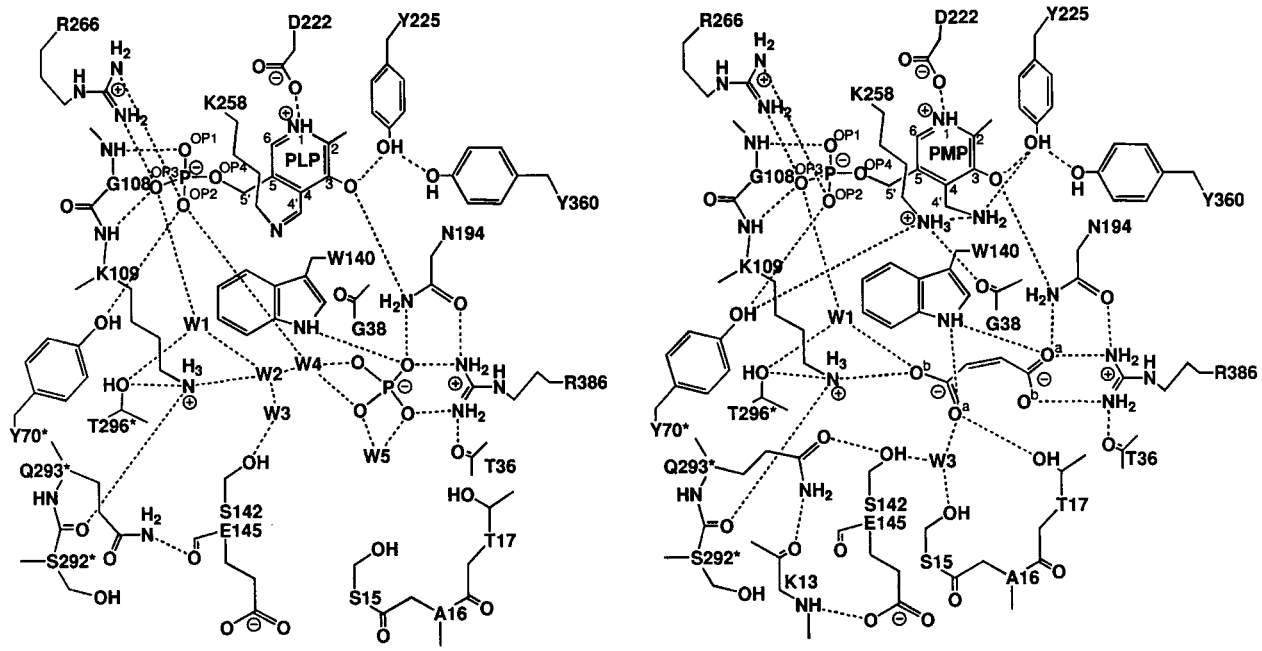

FIGURE 6: Schematic diagram showing hydrogen bond and salt bridge interactions of active site residues in the open (a, left) and closed (b, right) forms. Putative interactions are shown by dotted lines if the acceptor and donor are less than 3.5 Å apart.

OH of Thr296*, NH_3^+ of Lys109, W1, and W2 in the open form to form a salt bridge with the NH_3^+ of Lys109 and a hydrogen bond with W1. The phosphate moiety of the cofactor, OH of Thr296*, and the main chain C═O of Ser292* indirectly recognize the maleate through the cycle. The other carboxylate oxygen (Oa in Figure 6a) of the maleate participates in three hydrogen bonds with Trp140, Thr17, and W3. Ser142 and Ser15 indirectly recognize the maleate through W3. The amino group of PMP forms hydrogen bonds with the NH_3^+ of Lys258, the main chain C═O of Gly38, and the OH of Tyr225. The pyridine ring of PMP rotates by 12° toward the maleate at N1 of the pyridine ring as a pivot, compared with that of PLP in the open form. This rotation is attained by changing the dihedral angles around the linkage between C5 and the phosphate of the cofactor: OP1−P−OP4−C5′ = −87° (−33° in the PLP-type enzyme of the open form), P−OP4−C5′−C5 = 180° (−178°), and OP4−C5′−C5−C4 = 33° (−35°). The inclination angle between the pyridine ring of PMP and the indole ring is 5.3° (6.1° in the PLP-type enzyme), indicating that these two rings have the same relative orientation both in the PLP-type enzyme with the Schiff base between Lys258 and the cofactor and in the PMP-type enzyme without the Schiff base and rotate in cooperation. In eAspAT, the pyridine ring of PLP inclines about 17° toward Trp140 to achieve parallel stacking with the indole ring of Trp140.

The sequences of active site residues are 37% identical with those of eAspAT, which is markedly higher than the 16% identity of the total sequence. Especially, most of the important residues for the catalytic action around the cofactor are conserved between AspATs of subgroup Ia and tAspAT. These residues are Tyr70*, Trp140, Asn194, Asp222, Tyr225, Lys258, Thr296* (Ser in eAspAT), Tyr360 (Phe in eAspAT), and Arg386. The main chain atoms of these residues are superimposed within 1.30 Å with those of eAspAT, and the arrangements of the side chains around the cofactor are also well conserved between tAspAT and eAspAT. These results indicate that the stereochemistry of the catalytic mechanism in tAspAT is essentially the same as those proposed for the AspATs of subgroup Ia (*2*, *32*). Thr296* in tAspAT and Ser296* in eAspAT, pig cAspAT, and chicken mAspAT have strained main chain dihedral angles, and the role of residue 296* is conserved among them (*3*, *10*, *11*). The OH group of residue 296* interacts with the phosphate group of the cofactor through a water molecule in both the open and closed forms. Additionally, in the closed form, residue 296* participates in the recognition of the side chain carboxylate of the substrate through the water molecule. The possible participation of the residues with strained main chain dihedral angles in the protein function has been reported previously (*33*).

Substrate Recognition and the Role of Residues 36−38. There are two distinct differences in the active sites between tAspAT and eAspAT. One is concerned with the residues recognizing the side chain carboxylate of the substrate. In eAspAT, the guanidino group of Arg292* forms a salt bridge with the side chain carboxylate of the substrate. In tAspAT, no Arg residue corresponding to Arg292* was observed. Residue 292* in tAspAT is Ser. In place of Arg292*, Lys109 (Thr in eAspAT) forms a salt bridge with the side chain carboxylate of the substrate to compensate for the charge. In addition to this salt bridge, the carboxylate is directly hydrogen-bonded to W1, W3, Thr17, and Trp140 as shown in Figures 5b and 6b, indicating that the side chain carboxylate must be rigidly fixed for catalytic action as was observed in the AspATs of subgroup Ia (*3*, *9*−*14*). In both tAspAT and eAspAT, the side chains of the residues 17 and 18 occupy nearly the same positions of the active sites and interact with the substrate to cover the active pocket. In this sense, the roles of residues 17 and 18 are conserved. In aminotransferase subgroup Ib, residue 292 is Ser or Ala and residue 109 is Lys, indicating that Lys109 is the key residue for recognizing the side chain carboxylate of the substrate in subgroup Ib.

The other difference is concerned with the role of residues 36−38. The AspATs of many vertebrate enzymes and eAspAT have the consensus sequence of G36-H37-G38, where H is Leu or Val. G36, H37, and Gly37 approach the active site with a marked change in their main chain conformations and the side chain direction of H37 from the solvent region to the active site center. The side chain of H37 shields the substrate from the solvent region together with hydrophobic residues 17 and 18, and the main chain NH of Gly38 is hydrogen-bonded to the inhibitor (*3*, *9*−*14*). This conformational change is enabled by the presence of two glycines on both sides of H37. In tAspAT, the corresponding stretch is Thr36-Ala37-Gly38, suggesting that such a large conformational change is disallowed in this region because of the replacement of Gly36 by Thr. The stretch forming one side of the active site wall shows neither a significant change in conformation nor an approach to the active site on the binding of the maleate, resulting in the incomplete shield of maleate from the solvent region in the closed form. In the open form, the side chain of Thr36 faces the solvent region and its main chain C═O forms a hydrogen bond with the guanidino group of Arg386. In the closed form, Thr36 is enclosed in the protein interior by the access of α-helix H1 to the active site for its OH group to form hydrogen bonds with Asn21 of α-helix H1, keeping the interaction with Arg386. Thus, Thr36 might be one of the key residues responsible for the N-terminal movement. The side chain of Ala37 faces the solvent region in both the open and closed forms. The sequences of residues 36−38 of subgroup Ib shown in Figure 2 are divided into Thr36-Ala37-Gly38 and Gly36-H37-Gly38, where H37 is Ala or Ile. The latter stretch might behave in a manner different from the former in the substrate binding in AspATs of subgroup Ib.

Thermostability. The enzyme is stable up to about 80 °C at neutral pH. Some aspects of thermostabilty in tAspAT have already been described in terms of amino acid compositions (*5*). Here, tAspAT and eAspAT as a representative of mesophilic AspAT in subgroup Ia are compared in terms of surface, turns, and salt bridges to study the structural basis for thermostabilty, using the structures of the open form determined at 1.8 Å resolution. A more quantitative analysis related to thermostability must await the structure analysis of mesophilic AspAT in subgroup Ib, because the sequence identity between tAspAT and eAspAT is too low (16%), and even the overall structure of tAspAT is distinguishable from that of eAspAT (Figure 1).

The introduction of Pro residues into surface turns and loops has been well documented as an important stabilizing force in protein structure (*34*−*37*). The unusually high Pro content compared with that of mesophilic AspAT has been reported, and the distribition of most of the residues substituted with Pro in tAspAT on the molecular surface was pointed out on the basis of the tertiary structure modeled from the X-ray structure of eAspAT (*11*). In tAspAT, there are 25 Pro residues, of which three are located on α-helices, one is located on a β-sheet, nine are located on β-turns, and 12 are located on loops with all Pro residues at the β-turns or loops on the molecular surface, while there are 15 in eAspAT, of which two are on α-helices, two are on β-sheets, one is on a β-turn, and 10 are on loops. Pro rich tAspAT is characterized by eight β-turns containing Pro residues in contrast to one β-turn in eAspAT. Thus, the substituted Pro residues in β-turns might play some roles in the thermostability of this enzyme. The average ASAs of Pro residues on the molecular surfaces in tAspAT and eAspAT are 40.0 and 49.0 Å^2, respectively, indicating that the Pro residues in tAspAT are less exposed to the solvent region than those in eAspAT. The more buried hydrophobic Pro residues in the protein interior might be favorable for thermostabilty.

Ionic interactions play an important role in stabilizing protein structures (*34*, *38*−*40*). The charged area of the molecular surface in tAspAT is 2061 Å^2 larger than that in eAspAT (Table 2), and 73 and 51 salt bridges (distance cutoff of 4.0 Å) were observed in tAspAT and eAspAT, respectively, indicating a marked increase in the number of salt bridges in tAspAT compared with those in eAspAT. Out of 73 salt bridges, 53 are located on the molecular surface, implying that the salt bridges on the molecular surface stabilize tAspAT. Especially, the N-terminal arm in tAspAT is characterized by the three Arg residues (Arg2, Arg6, and Arg7). No such Arg was observed in the N-terminal arm of eAspAT. The deletion of the first to seventh or ninth residues in pig cAspAT causes critical damage to the enzyme activity, showing that the fixation of the N-terminal arm on the other subunit is very important (*41*). Arg2 and Arg6 form salt bridges with Asp197 and Asp113, respectively, to reinforce the interaction of the arm with the other subunit, probably contributing to the thermostabilty of tAspAT.

REFERENCES

1. Braunstein, A. E. (1973) *Enzymes 9*, 379−481.
2. Christen, P., and Metzler, D. E., Eds. (1985) *Transaminases*, Wiley, New York.
3. Jansonius, J. N., and Vincent, M. G. (1987) in *Biological Macromolecules and Assemblies* (Jurnak, F. A., and McPherson, A., Eds.) pp 187−285, Wiley, New York.
4. Mehta, P. K., Hale, T. I., and Christen, P. (1993) *Eur. J. Biochem. 214*, 549−561.
5. Okamoto, A., Kato, R., Masui, R., Yamagishi, A., Oshima, T., and Kuramitsu, S. (1996) *J. Biochem. 119*, 135−144.
6. Sung, M., Tanizawa, K., Tanaka, H., Kuramitsu, S., Kagamiyama, H., Hirotsu, K., Higuchi, T., and Soda, K. (1991) *J. Biol. Chem. 266*, 2567−2572.
7. Watson, R. J., and Rastogi, V. K. (1993) *J. Bacteriol. 175*, 1919−1928.
8. McPhalen, C. A., Vincent, M. G., and Jansonius, J. N. (1992) *J. Mol. Biol. 225*, 495−517.
9. Malashkevich, V. N., Strokopytov, B. V., Borisov, V. V., Dauter, Z., Wilson, K. S., and Torchinsky, Y. M. (1995) *J. Mol. Biol. 247*, 111−124.
10. Okamoto, A., Higuchi, T., Hirotsu, K., Kuramitsu, S., and Kagamiyama, H. (1994) *J. Biochem. 116*, 95−107.
11. Jäger, J., Moser, M., Sauder, U., and Jansonius, J. N. (1994) *J. Mol. Biol. 239*, 285−305.
12. Miyahara, I., Hirotsu, K., Hayashi, H., and Kagamiyama, H. (1994) *J. Biochem. 116*, 1001−1012.
13. Rhee, S., Silva, M. M., Hyde, C. C., Rogers, P. H., Metzler, C. M., Metzler, D. E., and Arnone, A. (1997) *J. Biol. Chem. 272*, 17293−17302.
14. McPhalen, C. A., Vincent, M. G., Picot, D., Jansonius, J. N., Lesk, A. M., and Chotia, C. (1992) *J. Mol. Biol. 227*, 197−213.
15. Nakai, T., Okada, K., Kawaguchi, S., Kato, R., Kuramitsu, S., and Hirotsu, K. (1998) *Acta Crystallogr. D54*, 1032−1034.
16. Sakabe, N. (1991) *Nucl. Instrum. Methods Phys. Res. A303*, 448−463.
17. Otwinowski, Z. (1993) *Data Collection and Processing*, *Proceedings of the CCP4 Study Weekend*, pp 56−62, Daresbury Laboratory, Warrington, England.

18. Collaborative Computational Project, Number 4 (1994) *Acta Crystallogr. D50*, 760−763.
19. Wang, B.-C. (1985) *Methods Enzymol. 115*, 90−112.
20. Bicogne, G. (1974) *Acta Crytsallogr. A42*, 142−149.
21. Jones, T. A., Zou, J.-Y., Cowan, S. W., and Kjeldgaard, M. (1991) *Acta Crystallogr. A47*, 110−119.
22. Navaza, J. (1994) *Acta Crystallogr. A50*, 157−163.
23. Brünger, A. T., Kuriyan, J., and Karplus, M. (1987) *Science 235*, 458−460.
24. Brünger, A. T. (1991) *Annu. Rev. Phys. Chem. 42*, 197−223.
25. Laskowski, R. A., MacArthur, M. W., Moss, D. S., and Thornton, J. M. (1993) *J. Appl. Crystallogr. 26*, 283−291.
26. Ovchinnikov, Y. A., Egorov, C. A., Aldanova, N. A., Feigina, M. Y., Lipkin, V. M., Abdulaev, N. G., Grishin, E. V., Kiselev, A. P., Modyanov, N. N., Braunstein, A. E., Polyanovsky, O. L., and Nosikov, V. V. (1973) *FEBS Lett. 29*, 31−34.
27. Doonan, S., Doonan, H. J., Hanford, R., Vernon, C. A., Walkar, J. M., Airoldi, L. P. D., Bossa, F., Barra, D., Carloni, M., Fasella, P., and Riva, F. (1975) *Biochem. J. 149*, 497−506.
28. Kabsch, W., and Sander, C. (1983) *Biopolymers 22*, 2577−2637.
29. Nicholls, A., Sharp, K., and Honig, B. (1991) *Proteins 11*, 281−296.
30. Gerstein, M., Lesk, A. M., and Chotia, C. (1994) *Biochemistry 33*, 6739−6749.
31. Mitchell, J. B. O., Thornton, J. M., Singh, J., and Price, S. L. (1992) *J. Mol. Biol. 226*, 251−262.
32. Kirsh, J. F., Eichele, G., Ford, G. C., Vincent, M. G., and Jansonius, J. N. (1984) *J. Mol. Biol. 174*, 497−525.
33. Herzberg, O., and Moult, J. (1991) *Proteins 11*, 223−229.
34. Vieille, C., and Zeilus, J. G. (1996) *Trends Biotechnol. 14*, 183−190.
35. Kawamura, S., Kakuta, Y., Tanaka, I., Hikichi, K., Kuhara, S., Yamasaki, N., and Kimura, M. (1996) *Biochemistry 35*, 1195−1200.
36. Matthews, B. W., Nicholson, H., and Becktel, W. (1987) *Proc. Natl. Acad. Sci. U.S.A. 84*, 6663−6667.
37. Kimura, S., Kanaya, S., and Nakamura, H. (1992) *J. Biol. Chem. 267*, 22014−22017.
38. Tanner, J. J., Hecht, R. M., and Krause, K. L. (1996) *Biochemistry 35*, 2597−2609.
39. Teplyakov, A. V., Kuranova, I. P., Harutyunyan, E. H., Vainshtein, B. K., Frommel, C., Hohne, W. E., and Wilson, K. S. (1990) *J. Mol. Biol. 214*, 261−279.
40. Kelly, C. A., Nishiyama, M., Ohnishi, Y., Beppu, T., and Birktoft, J. J. (1993) *Biochemistry 32*, 3913−3922.
41. Fukumoto, Y., Tanase, S., Nagashima, F., Ueda, S., Ikegami, K., and Morino, Y. (1991) *J. Biol. Chem. 266*, 4187−4193.
42. Kraulis, P. (1991) *J. Appl. Crystallogr. 24*, 946−950.
43. Burnett, M. N., and Johnson, C. K. (1996) Oak Ridge National Laboratory Report ORNL-6895, Oak Ridge National Laboratory, Oak Ridge, TN.

BI9819881